

AJP

ISSN : 0971 - 3093

Vol 28, Nos 10-12, October-December 2019

**ASIAN
JOURNAL OF PHYSICS**

An International Peer Reviewed Research Journal

Advisory Editors : W. Kiefer & FTS Yu

A Special Issue

Dedicated to

Prof Kehar Singh

Formerly Professor of Physics

at IIT Delhi

Guest Editor : R. S. Sirohi



ap

ANITAPUBLICATIONS

FF-43, 1st Floor, Mangal Bazar, Laxmi Nagar, Delhi-110 092, India

B O : 2, Pasha Court, Williamsville, New York-14221-1776, USA



Understanding dynamic beam shaping using liquid crystal spatial light modulator based binary holograms

Karuna Sindhu Malik, Nagendra Kumar, Akanshu Chauhan,
Nedup Sherpa and Bosanta R Boruah

Department of Physics, Indian Institute of Technology Guwahati, Guwahati-781 039, Assam, India

This article is dedicated to Prof Kehar Singh for his significant contributions to Optics and Photonics

In this paper, we describe wavefront shaping of a laser beam using a computer generated holography technique. We use liquid crystal spatial light modulator as a dynamic amplitude modulating device to implement binary holograms, which diffract an incident laser beam into a number of orders. The phase profiles of the diffracted beams have direct dependence on the description of the binary hologram, which on the other hand can be controlled in real time via a computer interface. Along with a brief theoretical background we present a proof-of-principle experiment to understand the working of binary hologram based beam shaping mechanism © Anita Publications. All rights reserved.

Keywords: Beam shaping, Liquid crystal spatial modulator, Binary hologram, Phase profile

1 Introduction

Shaping the wavefront of a laser beam is important for a large number of laser applications cutting across disciplines. In most of such applications the beam shaping needs to be performed in a dynamic fashion that is by using a reconfigurable beam shaping device. Liquid crystal spatial light modulator (LCSLM) provides a convenient way to modulate the beam via a computer interface [1]. Some LCSLMs can perform a direct phase modulation [2-4], where the zero order beam emerging from the device can get phase modulated. However, such modulation due to a limited range, and a strong dependence on the wavelength of the laser, is not suitable to provide an arbitrary shape to the wavefront. On the other hand, a laser beam incident on a binary hologram can get phase modulated into an arbitrary shape in one of the diffracted beams [5,6]. Such binary holograms can be implemented using an LCSLM [7] which performs a binary phase or amplitude modulation on the incident laser beam to achieve a user defined and arbitrary phase modulation in one of the odd order diffracted beams. Phase or amplitude binary holograms can be implemented by both nematic and ferroelectric LCSLM [5,7], whereas gray scale digital hologram can be implemented by nematic LCSLM only, which when implemented as a blazed grating can provide 100% (theoretical) diffraction efficiency. Digital holograms implemented using LCSLM have been shown to create arbitrary complex field [8] and to enhance our understanding on the interference phenomenon [9]. Besides LCSLM based digital holograms have been found to be extremely useful in the generation of various optical modes [10], including the orbital angular momentum (OAM) modes [11]. LCSLM based beam shaping has also found important use in optical imaging [12,13]. Application of LCSLM based beam shaping in optical trapping has led to the emergence of holographic optical traps [14,15]. The beam shaping using LCSLM has also been extended to high power lasers [16] and incident laser beam with several Watts of power was used for laser marking on thin film and metal surfaces [17].

Corresponding author

e-mail: brboruah@iitg.ac.in (Bosanta R Boruah)

Binary phase holograms can have a maximum diffraction efficiency of about $\sim 40\%$, which is less than the same of a blazed grating. However, binary holograms can be implemented using ferroelectric LCSLM which can have a display frame rate greater than 1 KHz; whereas nematic LCSLMs have a display frame rate of less than 200 Hz.

In this paper, we present a brief theory and a simple experiment to understand the phenomenon of wavefront shaping using an LCSLM based binary hologram. We begin with a discussion on the classical and binary holograms and show how binary hologram can generate not just one user defined wavefront but a number of such beams. We then illustrate design of a basic experimental arrangement to perform dynamic beam shaping using binary amplitude holograms. We discuss the experimental results and compare the same with numerical simulations to appreciate the efficiency of the scheme to generate a user defined wavefront in a laser beam.

2 Binarized computer generated holography

Figure 1 depicts the principle of classical holography. It involves two processes, namely the construction of the hologram and reconstruction of the object beam wavefront. In the former process, a laser beam is divided into two halves with one half illuminating an object and the other half, referred to as the reference beam, directed towards the plane where a holographic plate is kept. The beam reflected by the object, referred to as the object beam, carries the shape information of illuminated portion of the object in the form of a wavefront. The object beam and the reference beam meet at the holographic plate as shown in the Fig 1 (a), forming a stable interference pattern that gets recorded as the transmittance function of the recording plate. The developed holographic plate is called the hologram of the object being used. During the later process, the hologram is kept at the place in the same manner as the holographic plate was kept during the construction process. If the hologram is now illuminated with the same reference beam, it gives rise to three diffracted beams (assuming the object beam to be carrying only phase information) as shown in Fig 1 (b), called the undiffracted zero order beam which is the reference beam itself, the +1 order beam which is the reconstructed object beam and the -1 order beam which is the complex conjugate of the reconstructed object beam. The reconstructed object beam carries the same phase profile as the object beam during the construction process. As a result if one looks through the hologram towards the location of the object, one sees an image of the object at the same location even if the object is actually not present. This is due to the reason that the +1 order beam has a wavefront identical to the wavefront of the object beam. The principle of classical holography, therefore teaches us that an arbitrary wavefront can be created, provided the hologram with transmittance function proportional to the intensity in interference pattern between the reference beam and the object beam can be fabricated. One may in fact use a computer to obtain the interference pattern between a reference beam and a user defined object beam phase profile, and fabricate the corresponding hologram by some means such as using a digital printer or a photographic recording of a digital pattern. The above way of reconstructing the object beam is known as computer generated holography. The computer generated holograms can also be realized using LCSLMs or other spatial light modulators.

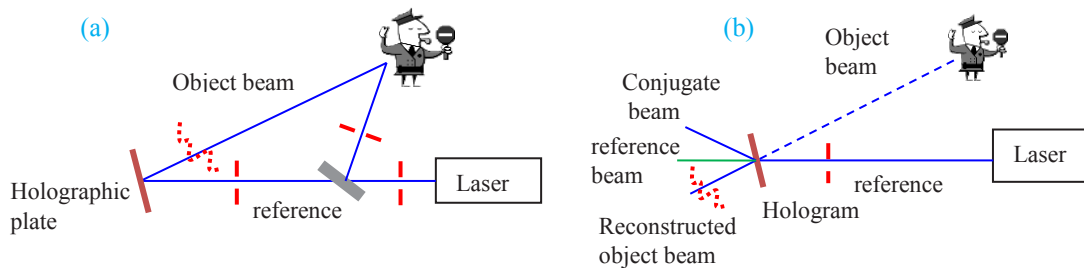


Fig 1. Illustration of (a) hologram construction and (b) object beam reconstruction in classical holography. The red dashed lines indicate the wavefronts.

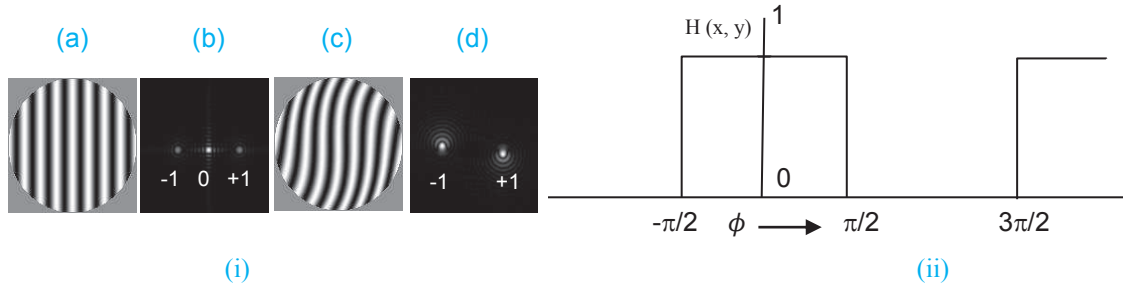


Fig 2. (i) Example of (a) an amplitude hologram (with the gray level indicating the amplitude transmittance) corresponding to a plane wavefront object beam and (c) a phase hologram (with the gray level indicating the phase delay introduced) corresponding to a coma aberrated object beam, resulting in a far field diffraction patterns as shown in (i) (b) and (d). (ii) Plot of transmittance function $H(x, y)$ vs the phase $\phi(x, y)$.

Figures 2 (i) (a) and **(c)** show two computer generated holograms using a tilted plane wavefront and a comatically aberrated and tilted wavefront as the object beam, respectively. The hologram in **Fig 2 (i) (a)** is an amplitude hologram while the hologram in **Fig 2 (i) (c)** is a phase hologram. The focal intensity distribution of the diffracted light from holograms in **Fig 2 (i) (a)** and **(c)**, can be computed using scalar diffraction theory [18]. Binary hologram is a binarized version (involving only two values) of the computer generated hologram. A binary hologram can be an amplitude hologram which comprises amplitude transmittance values of 1 and 0, or a phase hologram which introduces phase delays of 0 and π . Considering $e^{i\phi}$ to be the complex amplitude of the object beam in the hologram plane, the normalized transmittance function (neglecting any loss of light due to absorption) of the hologram for a plane reference wavefront parallel to the hologram plane can be written as $H(x, y) = 0.5(1 + \cos \phi(x, y))$, where (x, y) are coordinates in the hologram plane. In binary hologram, the transmittance value of the hologram is binarized using a threshold value of 0.5. Therefore, the transmittance function of a binary hologram for a plane reference wavefront parallel to the hologram plane can be written as

$$H(x, y) = \begin{cases} 1 & \text{if } \left(-\frac{\pi}{2} \leq \phi(x, y) \leq \frac{\pi}{2}\right) \\ 0 & \text{otherwise} \end{cases} \quad (1)$$

To understand how the light diffracted by a binary hologram carries the user defined phase information, we consider the plot of $H(x, y)$ vs ϕ at some generic location (x, y) , as shown in **Fig 2(ii)**. One may write using Fourier series analysis $H(x, y) = a_0 + a_n \cos(n\phi(x, y)) + b_n \sin(n\phi(x, y))$, where n is an integer,

$$a_n = \frac{2}{2\pi} \int_0^{2\pi} H(x, y) \cos(n\phi) d\phi \quad (2)$$

and

$$b_n = \frac{2}{2\pi} \int_0^{2\pi} H(x, y) \sin(n\phi) d\phi \quad (3)$$

Making substitutions for $H(x, y)$ using **Eq (1)** and **Fig 2(ii)**, we get

$$a_n = \frac{1}{n\pi} \left\{ \sin\left(\frac{n\pi}{2}\right) - \sin\left(-\frac{n\pi}{2}\right) \right\} \quad (4)$$

and $b_n = 0$. Therefore, barring the first term, $H(x, y)$ comprises only the odd indices of the second term. When the binary hologram diffracts a laser beam, each of the above odd indices gives rise to a diffracted beam referred to as diffraction order. Therefore, for a given odd order n , we may write,

$$H(x, y) = a_0 + \frac{1}{n\pi} \{ e^{in\phi(x, y)} + e^{-in\phi(x, y)} \} \quad (5)$$

In Eq (5), the first term corresponds to the undiffracted zero order beam while the second and the third terms correspond to the $+n$ and $-n$ order beams. Therefore, the $+1$ order beam carries the phase profile ϕ which was used to construct the binary hologram. Diffraction efficiency of the n^{th} order beam is given as $\{1/n\pi\}^2 \times 100\%$. The above derivation can easily be modified for binary phase holograms with $H(x,y) \times \pi$ as in Eq (1) representing binary phase delay introduced by the hologram. In this case the undiffracted zero order vanishes as $a_n = 0$, and the diffraction efficiency of the n^{th} order beam increases to $\{2/n\pi\}^2 \times 100\%$.

It is noticed that a binary amplitude hologram gives rise to a number of diffracted beams, which need to be well separated, if one wishes to utilize a particular order. Therefore, usually one expresses $\phi(x,y) = \phi_p(x,y) + \tau_x x + \tau_y y$, where ϕ_p is a pure phase variation defined with reference to a plane held normal to the propagation direction of the diffracted beam and (τ_x, τ_y) are tip and tilt expressed in the units of radian/length. Consequently the n^{th} order beam propagates in a direction indicated by $(n\tau_x, n\tau_y)$ relative to the zero order beam. Use of such tip and tilt helps one to isolate a given diffraction order from other orders using an iris diaphragm at the focal plane of the binary hologram.

The above scheme can also be extended to amplitude modulation in addition to phase modulation by coherently combining two uniquely modulated diffracted beams both having mutually orthogonal plane polarizations.

3 Implementation of binary holograms using an LCSLM

As stated already binary holograms can be implemented by both nematic and ferroelectric LCSLM, however, in this work we use nematic LCSLM only. Figure 3 (i) shows a representative display panel of a nematic LCSLM. It comprises of a two dimensional array of liquid crystal (LC) pixel with each pixel acting as an electrically addressable light modulator. Figure 3 (i) also shows the arrangement of a pixel in a transmissive type LCSLM. Each pixel contains liquid crystal sandwiched in between two alignment layers and transparent electrodes. Application of electric field across the pixel changes the polarization state of the transmitted light beam such that if an X polarized laser beam is incident on the LC pixel, the X polarized component of the emergent light is a function of the applied field. Electric field applied across each pixel can be individually controlled using a computer interface where a digital image sent to the LCSLM can be mapped to the voltages to be applied across the array of LC pixels. Therefore, a one bit image (i.e. black and white image) representative of the binary hologram can be sent to the LCSLM display panel, so that the device acts as a binary amplitude hologram for the given polarization state of the incident beam.

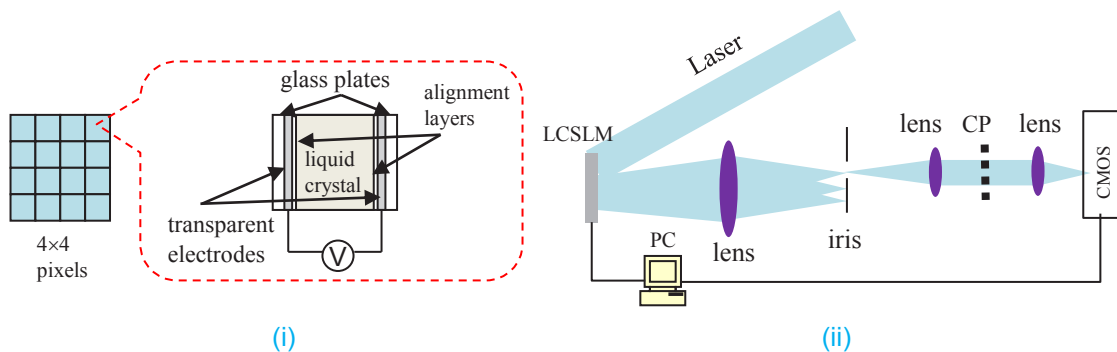


Fig 3. Illustration of (i) an LCSLM display panel, and (ii) the experimental arrangement.

In this work, we use a reflective type nematic LCSLM (Holoeye LC-R 720 , 1920×1200 pixels, pixel pitch = $8.1 \mu\text{m}$), where each LC pixel has a mirror on its back so that in lieu of the transmitted light, the reflected light gets amplitude modulated in accordance with the pattern displayed on the LCSLM panel. A schematic of the experimental arrangement is shown in Fig 3(ii). A collimated laser beam derived from a He-

Ne laser ($\lambda=633$ nm, maximum power = 13.5 mW) is incident on the LCSLM. Binary holograms described over 256 pixels computed by a Labview program in the PC are sent to the LCSLM panel. The light diffracted by the LCSLM is focused by a lens on an iris diaphragm. Choosing an appropriate combination of (τ_x, τ_y) one of the diffracted order can be passed through the iris to be recollimated by another lens. The two lenses can be arranged to form a 4f relay system such that the plane CP is optically conjugate to the LCSLM plane. Thus if phase ϕ_p is used to design the binary hologram, the phase in the plane CP is $n\phi_p$, if the iris transmits the n^{th} diffraction order. In this paper, we use Zernike mode representation of monochromatic aberration [19] and OAM modes to construct binary holograms. Figures 4 (a) & (b) show the color image representation of the phase profile of OAM modes with topological charge +1 and -1, respectively, while (c) and (d) show the respective binary holograms. We record the focal intensity distribution or focal spot of the given order by using another lens and a CMOS camera. It is also possible to split the incident laser beam into two by using a beam splitter to obtain a reference beam in addition to the beam incident on the LCSLM. The reference beam and the diffracted beam can interfere in the plane CP and the interference pattern can be recorded using the same CMOS camera.

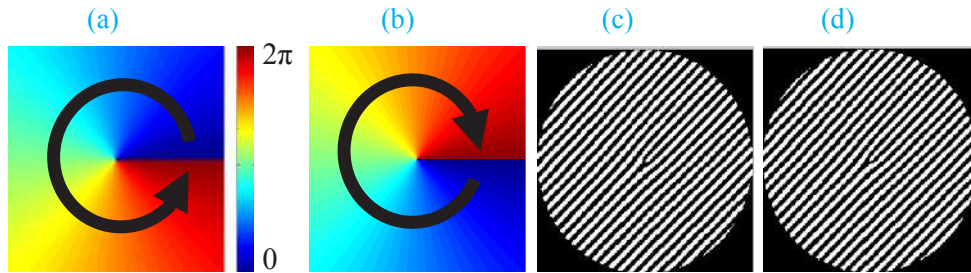


Fig 4. Phase profile of OAM modes with topological charge (a) +1 and (b) -1, and, (c) and (d) the corresponding binary holograms.

4 Results and Discussion

We first choose the combination of (τ_x, τ_y) so that the iris transmits the +1 order diffracted beam. The focal spot of the same as recorded by the camera is seen in Fig 5 (i) (a). It is noticed that the focal spot is not as symmetric as the Airy pattern which should be the focal spot of a beam with a circular pupil [18], due to the presence of astigmatism primarily contributed by the LCSLM itself. We then incorporate additional phase profile through ϕ_p which comprises primarily astigmatism, determined using brute force, so as to get a near perfect Airy pattern as seen in Fig 5 (i) (b). We then modify the binary hologram to incorporate OAM modes with topological charge +1, +2, +3 and +6 into the +1 order beam. Figures 5 (a) (ii), (iii), (iv) and (v) show the focal spots corresponding to topological charges +1, +2, +3 and +6, respectively, generated using scalar diffraction theory, while Figs 5 (b) (ii), (iii), (iv) and (v) show respective focal spots generated experimentally. We then modify the binary hologram to incorporate 1 radian (root mean square amplitude) of the Zernike modes representing coma and trefoil aberration modes. Figures 5 (c) (i) and (ii) show the theoretical focal spots corresponding to a beam carrying 1 radian of coma and trefoil, respectively, while Figs 5 (d) (i) and (ii) show the respective experimental focal spots. A comparison of the results shown in Figs 5 (a) and (b) confirms that the LCSLM based binary hologram is correctly generating the user defined phase profile in the +1 order beam. We then reduce the values of (τ_x, τ_y) by a factor of 1/3 so that the iris now transmits the +3 diffraction order. Figures 5 (d) (iii), (iv) and (v) show focal spots of the +3 order beam as recorded by the camera when the binary hologram is constructed using 1 radian trefoil, OAM mode with topological charge +1 and +2, respectively. Figures 5 (c) (iii), (iv) and (v) show theoretical focal spots corresponding to a beam with 3 radian trefoil, OAM mode with topological charge +3 and +6, respectively. Close resemblance of the

experimental and theoretical focal spot demonstrates that the +3 order beam carries a phase profile $3 \times \phi_p$ where ϕ_p is the phase profile carried by the +1 order beam.

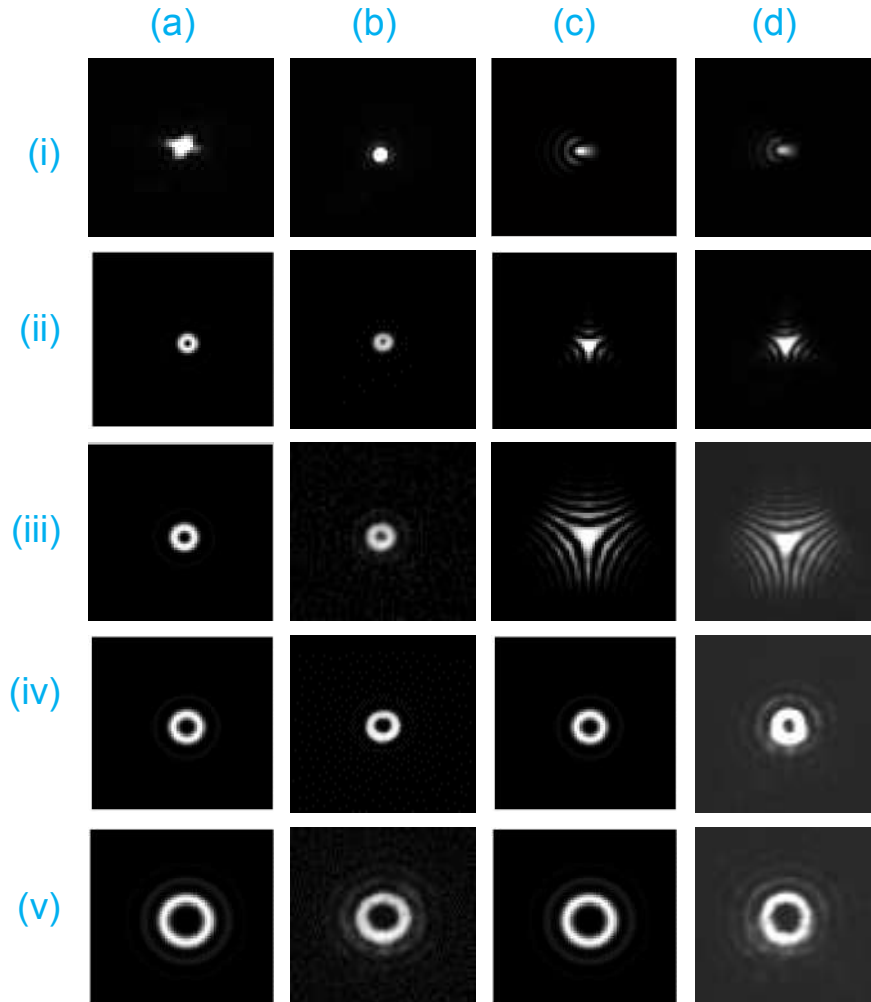


Fig 5. Experimentally obtained and theoretical focal intensity distributions corresponding to different phase profiles written onto the +1 order and +3 order diffracted beams.

To further analyse the quality of the phase profiles of the +1 order and the +3 order diffracted beams we also record the interference patterns between the diffracted beam and the reference beam in the plane CP.

Figure 6 (a) shows the interference of the +1 order beam corresponding to **Fig 5(i) (b)** and the reference beam while **Fig 6 (b)** shows the interference of the +1 order beam corresponding to **Fig 5 (ii) (b)** and the reference beam. We also record the interference of the +3 order beam corresponding to **Fig 5 (iv) (d)** with the same reference beam and the same is shown in **Fig 6 (c)**. Splitting of two interference fringes into three in **Fig 6 (b)** and one fringe into four in **Fig 6 (c)**, confirms that respective beam carries a topological charge +1 and +3.

It is, however, to be noticed that the diffracted beams and the reference beam may not have the same power, thereby requiring a neutral density filter to be placed in one of the beam paths.

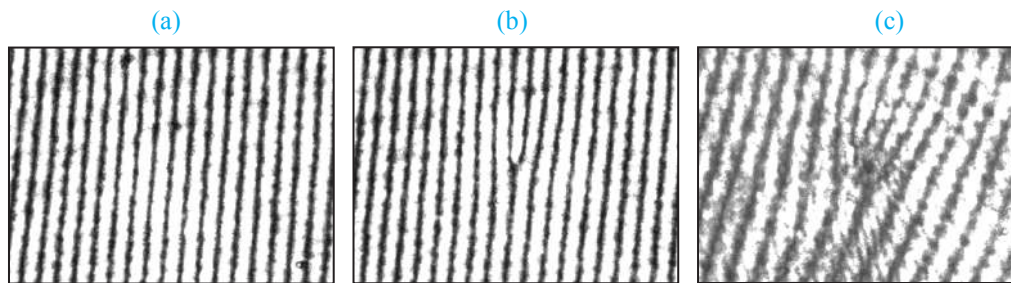


Fig 6. Experimental interference patterns (a) corresponding to the +1 order beam carrying only tip and tilt, (b) corresponding to the +1 order beam and (c) corresponding to the +3 order beam when the +1 order beam is designed to carry an OAM mode of topological charge +1.

5 Conclusion

In this paper, we have discussed the wavefront shaping using binary holograms. We described the principle behind analog phase modulation in a diffracted beam via a binarized version of a computer generated hologram. We showed how any odd order beam and not necessarily the +1 order beam, can carry user defined phase information. We have demonstrated the quality of the wavefront shaping in both the +1 order and +3 order beams using a simple experimental arrangement where the binary amplitude hologram is implemented using a reflective type liquid crystal spatial light modulator.

6 References

1. Efron U, Spatial light modulator technology: materials, devices, and applications, vol 47, (CRC Press), 1994.
2. Amako J, Miura H, Sonehara T, Wave-front control using liquid-crystal devices, *Appl Opt*, 32(1993)4323-4329.
3. Love G D, Wave-front correction and production of zernike modes with a liquid-crystal spatial light modulator, *Appl Opt*, 36 (1997)1517-1524.
4. Ostrovsky A S, Rickenstorff-Parrao C, Arrizon V, , Generation of the perfect optical vortex using a liquid crystal spatial light modulator, *Opt Lett*, 38(2013)534-536.
5. Neil M A A, Booth M, Wilson T, *Opt Lett*, Dynamic wave-front generation for the characterization and testing of optical systems, *Opt Lett*, 23(1998)849-1851.
6. Neil M, Wilson T, Juskaitis R, A wavefront generator for complex pupil function synthesis and point spread function engineering, *J Microsc*, 197(2000)219-223.
7. Boruah B R, Dynamic manipulation of a laser beam using a liquid crystal spatial light modulator, *Am J Phys*, 77(2009)331-336.
8. Dudley A, Majola N, Chetty N, Forbes A, Implementing digital holograms to create and measure complex-plane optical fields, *Am J Phys*, 84(2016)106-112.
9. Gossman D, Perez-Garcia B, Hernandez-Aranda R I, Forbes A, Optical interference with digital holograms, *Am J Phys*, 84(2016)508-516.
10. Forbes A, Dudley A, McLaren M, Creation and detection of optical modes with spatial light modulators, *Adv Opt Photonics*, 8(2016)200-227.
11. Cofre A, Garcia-Martinez P, Vargas A, Moreno I, Vortex beam generation and other advanced optics experiments reproduced with a twisted-nematic liquid-crystal display with limited phase modulation, *Eur J Phys*, 38(2017)014005; doi.org/10.1088/1361-6404/38/1/014005.
12. Tsai T.-H, Yuan X, Brady DJ, Spatial light modulator based color polarization imaging, *Opt express*, 23(2015)11912-11926.
13. Guo K, Bian Z, Dong S, Nanda P, Wang Y M, Zheng G, Microscopy illumination engineering using a low-cost liquid crystal display, *Biomed Opt express*, 6(2015)574-579.

14. Bhebhe N, Williams P A, Rosales-Guzman C, Rodriguez-Fajardo V, Forbes A, A vector holographic optical trap, *Sci Rep*, 8(2018)17387; doi: 10.1038/s41598-018-35889-0.
15. Gupta D K, Tata B, Ravindran T, Optimization of a spatial light modulator driven by digital video interface graphics to generate holographic optical traps, *Appl Opt*, 57(2018)8374-8384.
16. Li S, Ding L, Du P, Lu Z, Wang Y, Zhou L, Yan X, Using the spatial light modulator as a binary optical element: application to spatial beam shaping for high-power lasers, *Appl Opt*, 57(2018)7060-7064.
17. Parry J P, Beck R J, Shephard J D, Hand D P, Application of a liquid crystal spatial light modulator to laser marking, *Appl Opt*, 50(2011)1779-1785.
18. Goodman J W, Introduction to Fourier optics, (Roberts and Company Publishers), 2005.
19. Noll R J, Zernike polynomials and atmospheric turbulence, *J Opt Soc Am*, 66(1976)207-211.

[Received: 16.11.2019; accepted: 10.12.2019]